AD_____

Award Number: W81XWH-04-1-0239

TITLE: Early Detection of Breast Cancer by Fluorescence Molecular Tomography

PRINCIPAL INVESTIGATOR: Vasilis Ntziachristos, Ph.D.

CONTRACTING ORGANIZATION: Massachusetts General Hospital
Boston, MA 02114

REPORT DATE: Jul 2007

TYPE OF REPORT: Final

PREPARED FOR: U.S. Army Medical Research and Materiel Command
Fort Detrick, Maryland 21702-5012

# REPORT DOCUMENTATION PAGE

*Form Approved*
*OMB No. 0704-0188*



| **1. REPORT DATE** *(DD-MM-YYYY)* | **2. REPORT TYPE** | **3. DATES COVERED** *(From - To)* |
|---|---|---|
| 31-07-2007 | Final | 1 Jul 2004-30 Jun 2007 |

**4. TITLE AND SUBTITLE**

Early detection of breast cancer by fluorescence molecular tomography

**5a. CONTRACT NUMBER**

**5b. GRANT NUMBER**
W81XWH-04-1-0239

**5c. PROGRAM ELEMENT NUMBER**

**6. AUTHOR(S)**
Vasilis Ntziachristos, Ph.D.

E-Mail: vasilis@helix.mgh.harvard.edu

**5d. PROJECT NUMBER**

**5e. TASK NUMBER**

**5f. WORK UNIT NUMBER**

**7. PERFORMING ORGANIZATION NAME(S) AND ADDRESS(ES)**

Massachusetts General Hospital
Boston, MA 02114

**8. PERFORMING ORGANIZATION REPORT NUMBER**

**9. SPONSORING / MONITORING AGENCY NAME(S) AND ADDRESS(ES)**
U.S. Army Medical Research and Materiel Command
Fort Detrick, Maryland 21702-5012

**10. SPONSOR/MONITOR'S ACRONYM(S)**

**11. SPONSOR/MONITOR'S REPORT NUMBER(S)**

**12. DISTRIBUTION / AVAILABILITY STATEMENT**
Approved for Public Release; Distribution Unlimited

**13. SUPPLEMENTARY NOTES**

**14. ABSTRACT**
Molecular targeting approaches have tremendous potential for early-detection because they rely on elucidation of abnormal gene-expression, rather than on discovery of retarded anatomical changes inflicted by growing tumors upon their microenvironment. We investigated whether fluorescence molecular tomography (FMT) could be used to detect breast cancer at its earliest stages via the detection of injected, protease-activatable molecular probes. We have successfully completed all goals and achieved the three major aims of the proposal, i.e. i) the development of appropriate fluorescence imaging methods for highly reliable and quantitative fluorescence imaging ii) the establishment and imaging of appropriate animal models of spontaneous breast cancer that closely resembles human disease as a pre-clinical stage to clinical translation and finally iii) generated predictions on clinical utility by simulations and phantom measurements based on the in-vivo findings from the animal studies. It is demonstrated for the first time that molecular based detection of breast cancer is possible based on fluorescent signatures using fluorescence probes. This shift the paradigm of breast cancer detection, treatment monitoring and follow up of disease progression in clinically relevant settings.

**15. SUBJECT TERMS**
Molecular imaging, fluorescence, tomography, early detection, specificity, breast cancer

| **16. SECURITY CLASSIFICATION OF:** | | | **17. LIMITATION OF ABSTRACT** | **18. NUMBER OF PAGES** | **19a. NAME OF RESPONSIBLE PERSON** |
|---|---|---|---|---|---|
| | | | | | USAMRMC |
| **a. REPORT** | **b. ABSTRACT** | **c. THIS PAGE** | | | **19b. TELEPHONE NUMBER** *(include area code)* |
| U | U | U | UU | 34 | |

**Standard Form 298 (Rev. 8-98)**
**Prescribed by ANSI Std. Z39.18**

**Table of Contents**

# Introduction

Breast cancer is the second most common female malignancy in the United States. The ability to detect malignancies in their earliest stages is of tremendous importance. Early detection has been shown to increase likelihood of survival [1, 2] and to reduce the risk of disease recurrence[3-6]. However, early detection continues to be a significant diagnostic challenge and thus remains the focus of attention of a number of medical research groups.

Well-established detection techniques, most notably mammography, remain limited in their sensitivity to small-volume disease. Though mammography has been of great importance for detection of breast malignancies, many tumors have evaded detection by this method largely due to its limited contrast. The technique is particularly hampered by background interference such as increased tissue density or scarring from prior surgery. Functional imaging, which includes Magnetic Resonance Imaging (MRI) and Positron Emission Tomography (PET), has been used as a compliment to anatomical imaging and has shown significant potential to image functional characteristics of tumors [7]. However, the high cost and complex operational logistics of these modalities may limit their practicality for use in large-scale screening studies.

An additional parameter that plays a vital role in breast cancer detection is the ability to detect specific disease signatures based on the molecular profile of the disease. Molecular imaging, i.e., imaging of cellular and sub-cellular processes that are associated with molecular onset and evolution of disease, can lead to increased sensitivity and specificity and can improve the overall performance of a diagnostic study. Improved specificity, based on the detection of molecular profiles, can lead to the overall reduction in unnecessary biopsies, which are associated with increased healthcare costs and patient distress, and thus can lead to personalized medicine. It is foreseen that such methods will help optimize therapeutic strategies and will enable the effects of treatment to be more closely followed in time scales of hours or days instead of the longer timeframe of weeks or months that is the current standard for on anatomical imaging methods. Some of our recent review articles [8] [9] provide more detailed discussions of molecular imaging in general, and one of our recent studies [10] demonstrates the ability of optical imaging to visualize disease response.

Optical methods have emerged as economic, safe, and effective alternatives for functional imaging. Diffuse Optical Tomography (DOT) has been developed for imaging of breast cancers because of its ability to non-invasively quantify oxy- and deoxy-hemoglobin concentrations, which can be used to characterized angiogenesis and hypoxia [11-14]. In addition, DOT has been used in combination with MRI to detect tumors based on the extrinsically-administered contrast agent Indocyanine Green (ICG) that marks angiogenesis and permeability. However, these markers, though they enable DOT to effectively image well-developed tumors, are not ideal for detection of the earliest stages of disease. Consequently, while DOT may certainly be a useful tool for evaluating larger tumors, a more effective optical modality is needed for early detection.

Fluorescence Molecular Tomography (FMT) is a relatively new optical tomographic imaging approach that capitalizes on the strengths of molecular imaging. It bases detection on specific molecular signatures, using highly targeted fluorescent probes, rather than on anatomical or functional changes within tumor microenvironments. This approach yields a shift in the radiological paradigm that has traditionally focused on anatomy and physiology. Unlike DOT, FMT can three-dimensionally resolve protein expression, protease activity, receptor regulation, and similar molecular markers that play vital roles in carcinogenesis. It has been demonstrated in-vivo that NIR photons can penetrate more than 12 centimeters into the breast, and that fluorochromes accumulating in small tumors are detectable through the human breast[15]. We have previously shown that FMT is capable of resolving phantoms placed less than 1 mm apart [16]. More recently it has been shown that the technique can visualize apoptosis as a response to treatment[10]. Furthermore, because non-ionizing radiation is used, the technology allows for repeated imaging for screening or monitoring of disease. FMT thus holds great promise for early detection of breast malignancies.

At the time of our grant proposal, several elegant targeted fluorescent probes had already been developed [17] [18]for use with optical methods such as FMT. Among the most notable of these were the so-called "smart" probes (also termed "activatable probes"), which are optically silent until they interact with a specific enzyme, such as a protease, which then activates the probe, converting it to a brightly fluorescent state [19]. These probes are powerful not only because of their specificity for cancer-associated enzymatic activity, but also because they significantly minimize background levels and exhibit several-fold amplification of fluorescence upon activation, enabling dramatic improvements in signal-to-noise contrast. Because activatable probes fluorescence only in the presence of specific tumor phenotypes, they can easily be localized and quantified against a virtually "dark" background, allowing for highly sensitive and specific detection.

Our proposal suggested using a smart probe that is activated by major cathepsins, which are members of the cysteine family of proteases and play a central role in tumorigenesis and matrix invasion [20-22]. For example, it has been demonstrated that high levels of cathepsin B expression correlates positively with aggressive behavior and progression of human tumors and negatively with patient survival [20]. We therefore chose to evaluate the performance of this probe for imaging breast cancer development and progression.

Until the study was supported by this grant, in-vivo imaging of such probes were limited to basic feasibility studies, generally involving imaging of xenographic implants in nude mice. Generally, it was unknown how early in disease progression such probes could be used to reliably detect malignancies, as the in-vivo sensitivity limits of FMT have not been rigorously explored. The goals of our proposal were primarily (1) to develop and optimize optical technology for highly sensitive detection; and (2) to evaluate the early-detection limits of FMT by conducting a blind screening study of transgenic mice that develop spontaneous tumors of the mammary fat pad, closely mimicking the natural development and progression of human breast cancer. We

proposed developing imaging tools designed to systematically reduce background noise levels and to improve fluorochrome localization and quantification. The study was designed to investigate screening efficacy and to predict sensitivity limits of human breast cancer.

The hypothesis of this proposal is that highly sensitive fluorescence imaging (tomosynthesis) of molecular contrast will enable earlier detection of breast tumors based on signals associated with tumor growth and matrix invasion. We predicted that this technology could achieve high detection specificity.

Our study had three major goals:

Aim 1. *To develop appropriate photon illumination and detection strategies and reconstruction methods for highly sensitive fluorescence detection and quantification.*

Aim 2. *To utilize optimal photon technology from Aim 1 to study in-vivo detection of spontaneous disease in transgenic mice and to follow local disease progression and distant metastases.*

Aim 3. *To translate the animal study findings into clinically-relevant detection schemes.*

The first of these aims was designed to find an optimal illumination technology and processing method in order to obtain the highest detection sensitivity of fluorochromes in tissues. We proposed investigating limited angle projections versus multi-angle illumination, planar illumination, and transillumination schemes.

The second aim focused on the clinical relevance of FMT. We proposed a screening study involving transgenic mice that spontaneously develop breast tumors. Our interest was and continues to be primarily (1) to characterize detection capacity as a function of disease progression and tumor growth; and (2) to quantify fluorescence concentration in-vivo and determine whether it correlates with tumor expression profiles. This screening study would enable us to establish early-detection limits.

The third aim was to translate the copious data acquired from exploring the first two aims into an evaluation of the clinical feasibility of FMT for early-detection of breast cancer.

In the grant proposal we presented a timeline for accomplishing our primary aims for years 1 – 3 of the study (Table 1).

Table.1 Overview of aims and time line

| | Year 01 | Year 02 | Year 03 |
|---|---|---|---|
| **Aim 1: Method Development & Optimization** | | | |
| • Construction of 4-mode imaging chamber | X | | |
| • Developing imaging algorithms | X | | |
| • Optimizing imaging parameters with phantoms | X | | |
| • Optimize imaging parameters with orthotopic mouse model(s) | | X | |
| **Aim 2: In vivo Screening study** | | | |
| • Establish appropriate transgenic mouse model(s) | X | | |
| • Breed and screen mice for early detection of tumors | | X | X |
| • Study local and distant disease progression. | | X | X |
| **Aim 3: Clinical translation** | | | |
| • Construction of breast-like phantoms | | X | X |
| • Experiments with phantoms | | | X |
| • Simulations | | | X |

We have successfully completed all goals The following sections provide a detailed description of the progress achieved in the past three years.

## AIM 1: METHOD DEVELOPMENT & OPTIMIZATION

### Construction of four-mode imaging chamber

We successfully completed construction of a 4-mode, integrated illumination/detection small animal imaging system. A schematic of which is presented in Figure 1. This system was based on a previously-reported scanner [16] with key advancements to accommodate all four illumination schemes that were described in the grant proposal, namely *reflectance imaging, transillumination, tomosynthesis,* and *tomography.*

*Reflectance Imaging* The illumination branch (Figure 1, f, g) illuminates the animal through the chamber window, and reflected intrinsic or fluorescence photons are recorded on the CCD using band-pass filters. Figure 2 presents schematically the front-illuminating arrangement implemented.

*Transillumination*. In this mode, each of the 46 source fibers directed toward the back of the imaging chamber (Figure 1, e and Fig.2) is sequentially switched on and the transmitted pattern is filtered with appropriate intrinsic or fluorescence

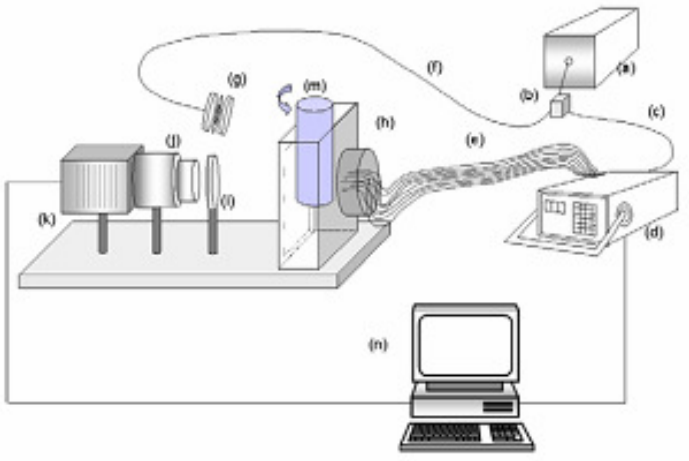


**Figure 1:** FMT imaging system.

band pass filters, and photons are recorded on the CCD camera. The resulting images are added together to create a composite image, which is geometrically similar to an X-ray mammogram. The fluorescence composite image may also be divided by the intrinsic composite image to generate a normalized image, which significantly reduces sensitivity to background heterogeneity and thus provides a more accurate image. In the *second year* we further upgraded this system in a fiber-free implementation by using motor stages to translate a single optical fiber emitting light focused on the animal surface, thus implementing significantly higher illumination versatility.

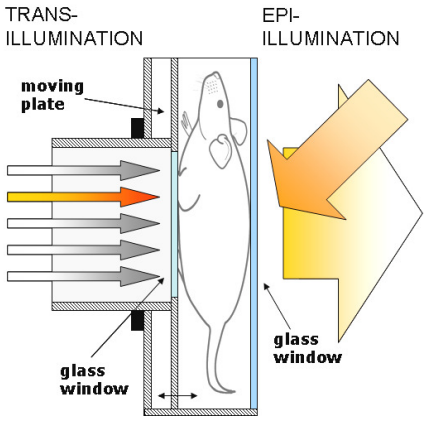


**Figure 2:** Detail of the imaging chamber shown in Fig.1 and modes of illumination.

*Tomosynthesis*. Limited angle projection FMT was further implemented, serving as FMT equivalent of tomosynthesis. For this approach data is gathered in the same manner as in the transillumination approach; however, unlike transillumination, tomosynthesis involves applying algorithms to the data that solve a volume integral equation relating spatially-distributed fluorochrome concentrations (in physical units) to the transillumination measurements. This offers more accurate quantification compared to transillumination.

*Tomography*. To achieve superior imaging performance it is important to illuminate using a large number of projections and detect signal around the animal, similarly to other tomographic techniques such as X-ray CT, PET or SPECT. For this reason we have implemented the rotational device (Figure 1, m and Fig.3) which rotates the object of interest in front of the illumination path and CCD camera to implement a number of projections. In this mode data can be collected in $360^0$ projections and offer true three-dimensional tomographic imaging.

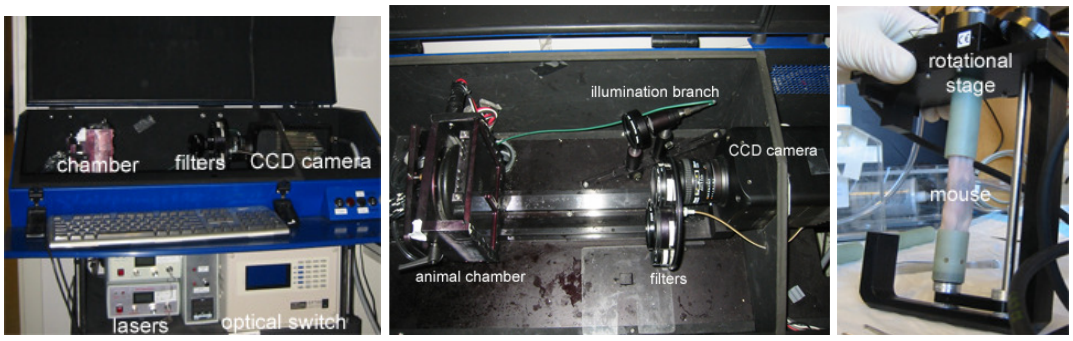


**Figure 3**: Photograph of FMT imaging system (left), a close-up photograph of the system (middle), and a photograph of the rotational stage with a mouse in place in the holder (right), which can be placed into the imaging chamber for complete projection ($360^0$) geometry.

*Multi-spectral imaging*

Dual wavelength imaging was also developed for allowing the ability to simultaneously resolve and differentiate probe bio-distribution and activation. Simultaneous imaging of different functional and molecular characteristics *in-vivo* can offer complementary information and significantly improve the accuracy of the findings. This can be achieved by elucidating coupled pathways at the cellular and sub-cellular level. This is a significant development and very relevant to cancer imaging. Dual wavelength capability was achieved by the addition of an additional laser and set of filters. The selection of the wavelengths was done based on the commercial availability of efficient fluorescent dyes. We selected illumination at 671nm and 748nm to illuminate popular fluorochromes that are commercially available and are typically used in the synthesis of fluorescent probes, for example the Cy5.5 dye (Amersham, Piscataway, NJ) or AlexaFluor 680 dye (Invitrogen, Carlsbad, CA) for the 671 wavelength and AlexaFluor 750 dye (Invitrogen, Carlsbad, CA) 748nm. Illumination in both cases was performed with CW laser diodes (B&W Tek, Newark, DE) which are time-multiplexed using a 2x1 channel optical switch Fig.1(ix) (DiCon FiberOptics, Berkeley, CA). The output of this switch is connected to the motorized fiber and its output is focused on the animal surface. Photon detection is based on a 512x512 element cooled CCD camera (Roper Scientific, Trenton, NJ) coupled to a AF Nikkor 35mm, f/2.8D lens (Nikon, Melville, NY) which is focused on the chamber's detection window. The CCD detector offers quantum efficiency of 60\% or better for the spectral region of 370nm to 830nm and therefore it is well suited for multi-spectral application in the NIR.

3-cavity band-pass (Andover Optics, Salem, NH) and long-pass filters (Omega Optics, Brattleboro, VT) were used to effectively block excitation light an minimize cross-talk between fluorescent dyes while maximizing transmission at the selected wavelengths. Filters were also used for the excitation wavelengths. Laser diode signals were pre-conditioned with a 671DF10 bandpass filter (Omega Optics, Brattleboro, VT). Pre-filtering the laser to remove unwanted wavelengths and harmonics improved cross-talk by a 4 fold decrease. Excitation measurements were performed through bandpass filters (Andover Optics, Salem, NH). Emission data was collected through a combination of a long pass and band pass filter (Longpass filter: 695nm, bandpass 710nm +/-20nm for the Cy5.5 measurements and longpass filter: 770nm and bandpass at 800nm +/- 20nm for AF750 based measurements)

**Development of imaging algorithms**

In the course of the proposal we developed tomographic algorithms that fundamentally improve the accuracy of fluorescence imaging based on photon propagation models in tissues. In particular, we developed imaging algorithms for trans-illumination as well as advanced background fluorescence subtraction techniques (reported in Ref. [23]). We also evaluated algorithms for robust imaging within highly heterogeneous backgrounds, suitable for in-vivo imaging [24, 25]. Lastly, we adapted algorithms already designed for tomosynthesis to complete-projection imaging [26]. Through implementation of several phantom studies, we then evaluated the developed algorithms in order to assess the overall performance of the method. We specifically constructed highly heterogeneous phantoms (of solid and liquid diffusive media), intended to best simulate the varying optical properties that are likely within breast tissue.

The tomographic approach employed was based on a self-calibrated algorithm for diffuse fluorescence reconstructions developed specifically for imaging fluorochrome distribution in-vivo. The algorithm has been implemented into functional code using Matlab on a personal computer and is based on previously developed analytical solutions for fluorescence propagation in diffuse media. In its general form, the algorithm constructs a synthetic measurement $U_s(\vec{r}_s,\vec{r}_d)$ detected at position $\vec{r}_d$ due to a source at position $\vec{r}_s$, which is written as

$$U_s(\vec{r}_s,\vec{r}_d)=S_0\cdot\frac{U_{fl}(\vec{r}_s,\vec{r}_d)-U_{bl}(\vec{r}_s,\vec{r}_d)}{U_{inc}(\vec{r}_s,\vec{r}_d)}=\frac{1}{U_0(\vec{r}_s,\vec{r}_d,k^{\lambda 1})}\int d^3r\cdot(U_0(\vec{r}_s-\vec{r},k^{\lambda 1})\cdot n(\vec{r})\cdot\frac{\upsilon}{D^{\lambda 2}}G(\vec{r}_d-\vec{r},k^{\lambda 2}) \quad (1)$$

where $U_{fl}(\vec{r}_s,\vec{r}_d)$, $U_{inc}(\vec{r}_s,\vec{r}_d)$ are measurements at the emission and excitation wavelength respectively, $U_{bl}(\vec{r}_s,\vec{r}_d)=\Theta_f\cdot U_{inc}(\vec{r}_s,\vec{r}_d)$ is the bleed through signal, $\Theta_f$ is the band-pass filter attenuation factor, $S_0$ is a gain term that accounts for instrument gain differences at the excitation ($\lambda_1$) and emission ($\lambda_2$) wavelengths, $n(\vec{r})$ is the product of the fluorochrome absorption coefficient and fluorescence quantum yield, $k^{\lambda 1}, k^{\lambda 2}$ are the wave propagation vectors at $\lambda_1$ and $\lambda_2$ respectively, $\upsilon$ is the speed of light into the medium, $D^{\lambda 2}$ is the diffusion coefficient at the $\lambda_2$, $U_0(\vec{r}_s-\vec{r},k^{\lambda 1})$ is a term that theoretically describes the established photon field at position $\vec{r}$ into the medium at $\lambda_1$ and $G(\vec{r}_d-\vec{r},k^{\lambda 2})$ is a term that describes the propagation of the emission photon wave from a fluorochrome at position $\vec{r}$ to the detector.

The terms $U_0$, $G$, also referred to as the "forward model", are calculated analytically or numerically. Both analytical and numerical-differences methods for obtaining the functions $U_0$ and $G$ are currently available in our laboratory for two- and three-dimensional forward problem and for arbitrary boundaries. The calculation of these functions with complex boundaries, based on the Kirchhoff approximation, and for non-contact measurements has been published. Eq.1 is typically discretized over the volume investigated and the discrete problem is then inverted or minimized. For reconstruction purposes algebraic reconstruction techniques, singular value decomposition and regularization or conjugate gradient methods are used. Experimentally, we have found the algebraic reconstruction technique and the statistical inversion method described in the following to perform optimally for breast cancer imaging.

*Implementation of non-contact measurements*

Lens-coupled CCD measurements, in contrast to fiber measurements (contact measurements), detect light from the body surface at angles that are not always normal to the surface. This is especially true for measurements performed without the matching fluid. In these cases it is required that the angle between the normal unit vector to the detector plane and the normal unit vector to the surface S of the diffuse medium or animal imaged is taken under consideration. Assuming a 3D boundary with a unit vector from the surface, the field actually

detected by the CCD camera can be written for the angle dependent expression for outward flux, which is written as a summation of all surface elements:

$$J_{\det}(\vec{r}_d) = \frac{1}{\pi}\sum_p J(\vec{r}_p)\Gamma(\vec{r}_p - \vec{r}_d)\Delta(\vec{r}_p) \tag{2}$$

where $J(\vec{r}_p) = -D\cdot\partial U^{KA}(\vec{r}_p)/\partial\hat{n}_p$ is the flux on the surface boundary at $\vec{r}_p$, $U^{KA}(\vec{r}_p)$ is the photon fluence calculated on the boundary at $\vec{r}_p$ using the Kirchhoff approximation [27]or higher order method[28, 29] and

$$\Gamma(\vec{r}_p - \vec{r}_d) = \frac{\exp(i\omega|\vec{r}_p - \vec{r}_d|/c)}{|\vec{r}_p - \vec{r}_d|^2}\xi(\vec{r}_p - \vec{r}_d)\cos\theta_p\cos\theta, \quad \cos\theta_p = \hat{n}_p\cdot\frac{(\vec{r}_d - \vec{r}_p)}{|\vec{r}_d - \vec{r}_p|}, \quad \cos\theta = \hat{n}\cdot\frac{(\vec{r}_p - \vec{r}_d)}{|\vec{r}_p - \vec{r}_d|},$$

(9)

where the term $\xi$ is the visibility factor, which is either unity if both points $\vec{r}_p$ and $\vec{r}_d$ can be joined by a straight line without intersecting the surface interface (i.e. when they are visible to each other), and where $\hat{n}$ is the surface normal of the detector where the flux $J_{det}$ is measured.

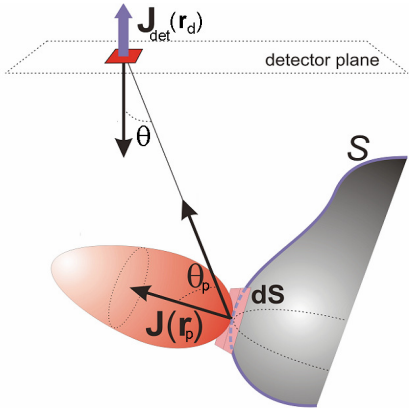


**Figure 4.** Geometry assumed in non-contact formulation

*Statistical inversion of the normalized Born*

Central to the ability of FMT to operate *in-vivo*, in the presence of significant optical heterogeneity is the use of the normalized Born (nBorn) approximation, i.e. a normalization scheme that divides fluorescence measurements with corresponding measurements after tissue illumination at the excitation (and possibly the emission) wavelength and similarly normalizes the theoretical model used for photon propagation (for method details See Refs. [30] [24]). In Ref. [24] we studied the nBorn accuracy, as a function of background optical heterogeneity, and found that up to 4x background attenuation changes (due to scattering or absorption), with size and spatial heterogeneity similar to that seen in tissues leads to less than 15% errors on the intensity of the reconstructed fluorescence activity on the FMT image and less than 7% on the reconstructed size of objects. Conversely the nBorn ratio comes with the significant shortcoming that very low intensities (or noise) at the excitation wavelength, combined with high values at the emission wavelength creates abnormally high ratio's and leads to noise or artifacts to appear in the images.

To account for the nBorn limitations, we have recently considered a statistical inversion scheme [31]. The underlying problem solved in this development is that although the individual measurements at each wavelength can be modeled with reasonable accuracy using the Gaussian approximation of the Poisson-distributed optical measurements, the ratio of two Gaussian random variables (RV's) produced by the nBorn ratio normalization does not lead to an easily tractable distribution. The most commonly known example is when both random variables are zero mean with unit variance, which leads to a Cauchy density. Introducing non-zero means complicates the distribution, and the density of the ratio does not lend itself to a simple

relationship between the data and the unknowns. We have therefore derived an approximation to the distribution of the nBorn value which involves repeated solution of an iteratively re-weighted conjugate gradient problem [31]. The weights in this formulation play the role of data-derived thresholds, automatically determined by the statistical model, based on the experimental signal to noise ratio (SNR) in the measurements. An approximate maximum likelihood solution can be derived from this statistical model, that takes the form of an iterative method, , $x^{n+1}=\zeta(x^n)$, where

$$\zeta(x^n)=[W^T Q(x)^T Q(x) W]^{-1}\left[\sum_i \frac{dg_i(u_i,x)}{dx}+W^T Q(x)^T Q(x)u-\left(\frac{dq(x)}{dx}\right)^T A(x)^T A(x)q(x)\right] \quad \text{Eq.1}$$

in which $Q(x),q(x)$ and $g(u,x)$ are functions that depend on statistical characteristics of the normalized Born data $u_i$ and effectively weight the sensitivity matrix W (forward model). Details on the derivation of functions $Q,q,g$ for this formulation are rather complex for detailed description in this section and are instead included in Ref. [32]. Here we showcase the effect of the equivalent thresholds calculated by this method on raw data obtained experimentally from an experimental Her2/neu animal, with a tumor visible on the upper torso of the animal, marked by an arrow in Fig.5. Fluorescent signals from the tumor following administration of a *cathepsin-sensitive fluorescent probe* described in Ref.[18] resolved increased presence of the enzyme in the tumor compared to the healthy mammary. Images from the control mouse (not shown here) did not show significant fluorescence activity. The large boxes on Fig.5 b,c indicate the detector FOV. Fig.5 b,c depict FMT (tomo-synthesis) images in color, obtained with an empirical threshold (b) vs. using the statistical inversion method (c). The statistical inversion shows image quality that is identical to the best tuned manual threshold showing a method appropriate for imaging fluorescence activity tomographicaly without the need for user input, i.e. automatically.

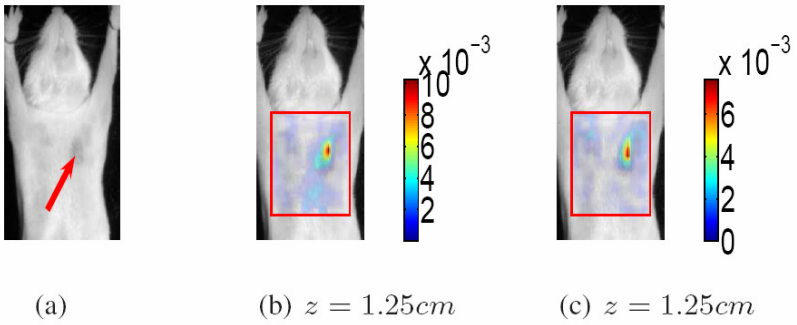


**Figure 5:** Photograph of a Her2/neu mouse positioned in the imaging chamber. The arrow indicates the presence of the tumor. (b) Fluorescence image in color reconstructed using user-defined thresholds, based on a cathepsin-sensitive activatable fluorescence probe superimposed on image (a). The image shows increased fluorescence and therefore cathepsin activity in the Her2/neu tumor. (c) the same image as in (b) reconstructed using automated thresholding via the statistical nBorn I nversion.

*Imaging at highly heterogeneous backgrounds*.

One of the common criticisms concerns the performance of optical methodologies in tissues with high background optical heterogeneity. Recently however it has been demonstrated that methods that employ fluorescence measurements normalized by corresponding signals obtained in the excitation wavelength are not sensitive to background optical heterogeneity [33,

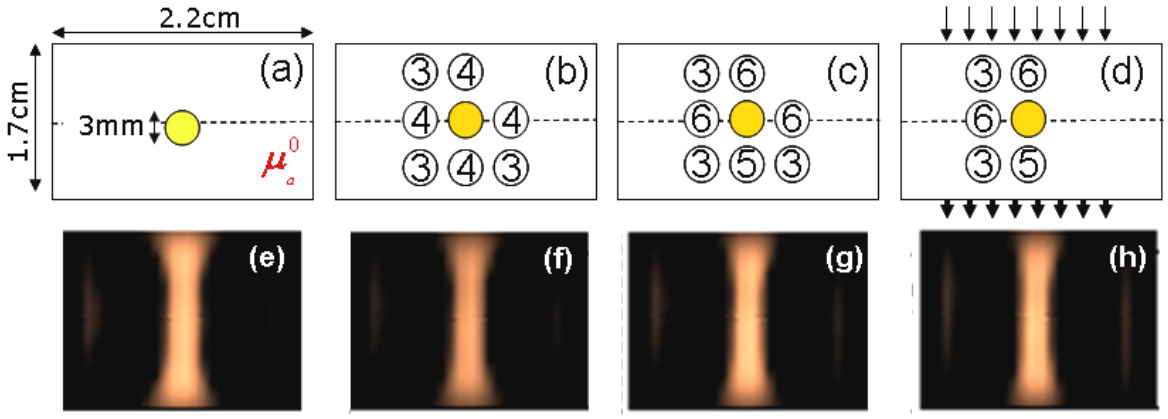


**Figure 6**: Imaging at highly heterogeneous backgrounds. (a)-(d) A fluorescent tube, representative of a tumor, was imaged at the presence of an increasing surrounding absorption. The numbers in the white circles indicate the absorption contrast of this tube relative to background (i.. 3x, 4x etc). (e)-(h) Images showing a slice passing from the middle of the chamber. In all cases the tube reconstructs very accurately despite the background absorption. The images showed a quantification variation of the order of 20% in this case.

34] [25]. We have previously proposed and adopted a normalized inversion technique because it yields computationally efficient reconstructions [30] . We further tested this method with highly heterogeneous backgrounds and one paper is now published with those findings [25].

Some of the most interesting results are summarized in Fig.6 where it can be seen that the method is very robust in reconstructing even at a high degree of background absorption heterogeneity. This study proves that the proposed methods are well suited for in-vivo imaging of mice or human breast, where high degree of background optical property variation is expected due to the close proximity of several organs or tissue structures with different optical properties.

## Phantom studies

In addition to the ones discussed already, we performed extensive phantom studies to evaluate algorithmic performance and assess the overall performance of the method. In particular we constructed optically heterogeneous phantoms using combinations of solid and liquid diffusive media and investigated the performance of the methods with a varying degree of heterogeneity and background fluorescence. In addition we streamlined the developed of resin phantoms, of different optical properties that can simulate tissues of different optical properties (for example varying optical properties in the breast due to aging); results that are now in press [35]. Some of the most relevant studies are described in some more detail in the following:

### *Imaging fluorochromes in diffusive media*

We undertook studies to compare the performance of planar and tomographic methods to quantify fluorochromes as a function of depth and optical properties. Here we summarize some of the most relevant and representative findings, from a significantly longer list of measurements and studies (some also shown in Fig.6).

One study compared planar imaging and tomosynthesis (tomographic) performance in a side by side comparison. Shown in Figure7a is imaging of two ~1.5mm diameter fluorescent tubes (500nM Cy5.5, 3mm apart) immersed at different depths in a water solution of intralipid and India ink simulating the optical properties of tissue. Both modalities resolve the tubes when placed superficially although FMT offers better resolution. However, detection becomes highly

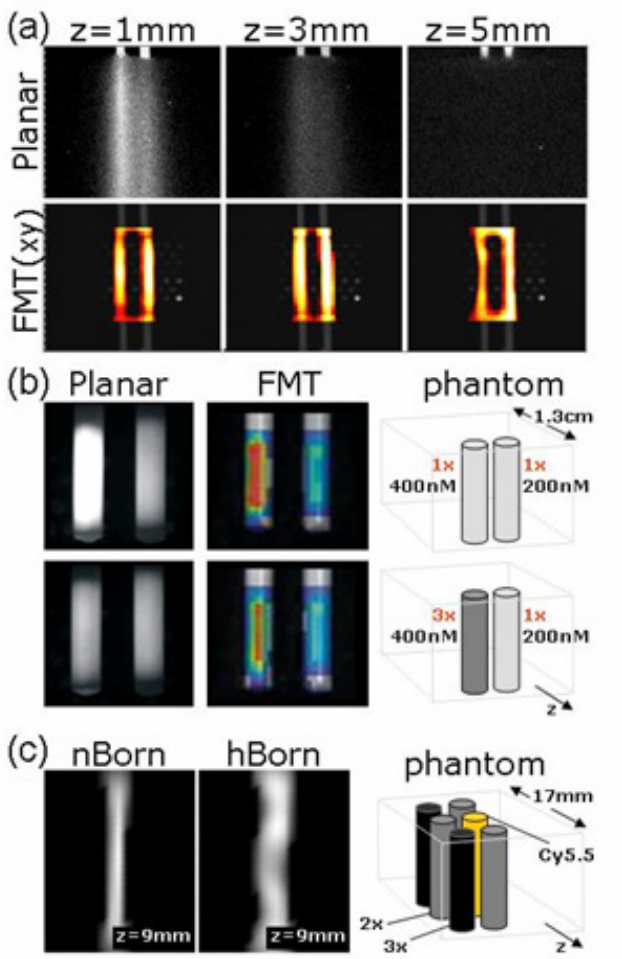


**Figure 7**: Side-by-side comparison of planar and tomographic imaging (a) as a function pf depth, (b) as a function of varying local optical properties, and (c) as a function of heterogeneity. In all cases tomosynthesis (tomography) is shown superior to planar imaging.

challenging as a function of depth for planar imaging with the tubes barely visible even 3mm deep. Depth sensitivity highly depends on the size and strength of fluorochrome, but the images contrast the superior ability of tomography to look deeper in diffuse media and with higher resolution, using in this case identical hardware to the one used for planar imaging. The color images are reconstructed slices obtained at different depths and superimposed on gray scale

photographs of the tubes for visualization purposes. Similar results are obtained in comparisons of transillumination and tomography, although transillumination can still record objects deeper than in planar imaging. Similarly, the ability to image fluorochromes with varying background optical properties is showcased in Figure 7b, which depicts planar and reconstructed images of two fluorescent tubes, the left tube containing double the amount of Cy5.5 in the right tube (400nM vs. 200nM). The tubes are immersed in the same diffuse fluid as in (a). Both techniques accurately resolve the 2:1 relation in fluorochrome concentration between left and right tubes when background absorption is the same in both tubes (top row). However when India Ink is added in the left tube to simulate a three-fold increase in vascularization (absorption), planar performance is significantly reduced, erroneously reporting a 1:1 Cy5.5 concentration in the two tubes (bottom row). This is because the added ink absorbs more fluorescent photons. In contrast tomography can correct for these phenomena and demonstrates more robust performance reporting 1.8:1 relation in this case. Finally, Figure 7c demonstrates the capacity of tomography to resolve a single fluorescent tube in the middle of a highly diffusive medium when it is asymmetrically surrounded by 5 strong absorbers of 2x and 3x the background absorption and of comparable sizes. This result demonstrates the robustness of tomography to image highly heterogeneous media, an ability that is mainly due to the data normalization techniques (image labeled nborn) employed tomographically. Absence of normalization results in distorted tomographic imaging performance (shown in the image labeled nBorn). Both images are slices from a three dimensional reconstruction obtained at 9mm depth. Planar imaging could not detect the presence of a fluorochrome in this highly absorbing and heterogeneous background.

Overall, these findings exemplify that planar (reflectance) imaging should be used with caution. Signal intensity relates linearly to fluorochrome concentration but non-linearly to depth, size and optical properties and is further complicated by the high scattering nature of tissue. Tomosynthesis and tomography have the potential to improve on these limitations and to offer more robust and accurate imaging.

*Algorithmic testing - statistical inversion*

The statistical inversion method described in the previous section concentrated on establishing a uniform basis from which to compute reconstructions. This allows for greater consistency between data sets, which in turn enables easier and more accurate analysis of the resulting images. It has been understood that by taking the ratio of emission over excitation signals, information about the noise in those signals is obscured, and intensity is no longer an appropriate indicator of signal to noise ratio (SNR). Because of this, highly noisy data points may be heavily weighted when using all data points to compute an image, resulting in a poor result. The previous solution to this dilemma was to remove data pairs from the inverse solution based on minimum signal thresholds for each of the fluorescence and excitation signals [30]. Data pairs were then removed from the reconstruction algorithm when one or both of the received signals failed to meet the minimum requirements. While effective, this method was highly variable, and required a considerable amount of user input in order to operate effectively. This increased the variability of the reconstructions, not only from one mouse to another, but even with regards to a single mouse imaged at different times. As such, direct comparison of

such reconstructions was more challenging. The direct inversion method was applied to *in-vivo* data as shown in Fig.5, but was first extensively tested in phantoms. One example imaging two fluorescent tubes at two different depths (z=0.42cm and z=1.25cm) is shown in Fig.5, immersed in a chamber containing an intralipid – India Ink solution with absorption coefficient of 0.2cm-1 and reduced scattering coefficient of 15cm-1. The tubes were made of semitransparent plastic, sealed on one end and containing the same intralipid – India Ink solution and 200nM of the Cy5.5 fluorescent dye.

By forming a maximum likelihood (ML) problem we obtained, similarly to the analysis that led to Fig.5, a solution which optimally weights each of the individual data points. The weighting of each raw datum collected is automatically determined based on the signal to noise characteristics of the measurement and requires no user input. Starting from the complete statistical problem statement, the constructed inversion approach is more reliable in handling various amounts of signal and noise in the data as shown in experiments from phantoms in intralipid (c.f Fig.8), euthanized mice with implanted tubes (not shown, but in Ref. [32]), and in-vivo imaging sessions (c.f Fig.5). In particular in Fig.8 it is shown that the best images that can be reached by manual data-threshold (5b, 5c), achieved by trial and error from a user, produces the same result as the automated method using statistical inversion (5e, 5f) The advantage that these new methods have is in their automated nature. Rather than requiring multiple inversions in order to determine the best threshold levels, our statistical methods need only be run once. Importantly it requires no user input that makes it a very robust approach for quantification studies in multiple animal and imaging sessions, such as the ones proposed herein; yet the resulting answer is of equal or better quality than those obtained using threshold methods, and is more consistent across multiple data sets.

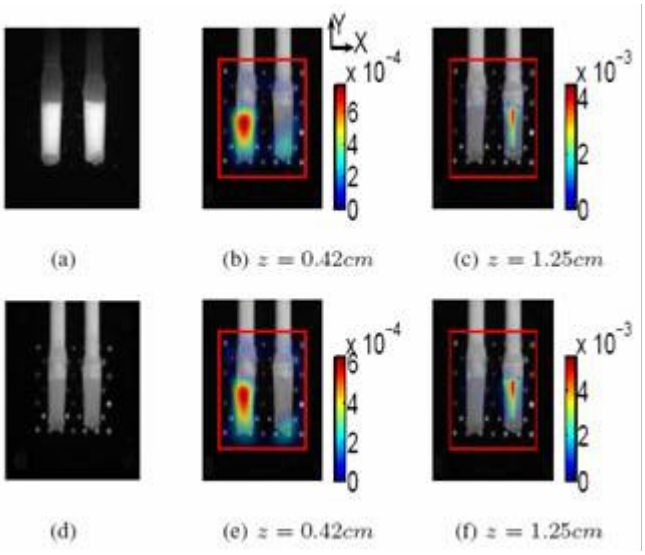


**Figure 8:** Dual Tube Phantom: (a) Reflectance Fluorescence image (b) Manual Threshold: Coronal slice through tube at z=0.42cm (c) Manual Threshold: Coronal slice through z=0.42cm (d) Flat image (e) Statistical inversion: coronal slice through z=0.42cm, (f) Statistical inversion: coronal slice through z=1.25cm. In all images, z=0cm corresponds to the source side, with total slab thickness of 1.3cm (c.f. Fig.2). The red box in the image denotes the boundary of the solution space.

*Algorithmic testing – dual-wavelength imaging*

We performed extensive characterization of the spectral separation ability of this system. A related result based on experimental phantom measurement is shown in Fig. 9. The figure shows two tubes placed in the system imaging chamber and photographed before the addition of intralipid with optical properties those of the human breast. The left tube contained 250nM of the Cy5.5 dye (emission max : 690nm) and 500nM of the AF750 dye (emission max : 770nm). The right tube contained 500nM of Cy5.5. and 250nM of AF 750. The fluorescence appearance of the tubes, when imaged with the dual wavelength FMT system clearly shows the 1:2 and 2:1 ratio when the tubes are imaged at the Cy5.5. (top row) and AF750 channel (bottom row) is shown in the middle column marked "FRI", which is a fluorescence photograph of the tubes in he absence of a surrounding diffusive material . Finally, FMT images after the tubes were immersed in a highly-diffusive breast-like fluid also demonstrated the same separation. In all cases the cross-talk between the two channels was found to be less than 1% using the filter combination described above.

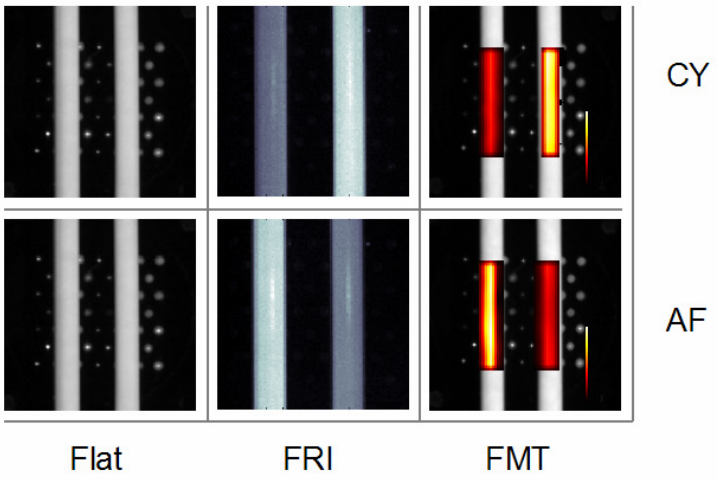


**Figure 9:** Separation of fluorochromes at different wavelengths using the dual wavelength system . (see text for details)

*Algorithmic optimization and testing – in-vivo studies* A total of 8 mice, from a significantly larger pool of animals imaged in-vivo, served to produce *training sets* for data optimization. Our development of the statistical inversion method for automatic setting of data parameters required no algorithmic optimization in the "traditional" sense, i.e. by trial and error. Instead this training set was used to confirm that the measurements and corresponding predictions of noise models, necessary in the operation of the statistical inversion method, that was

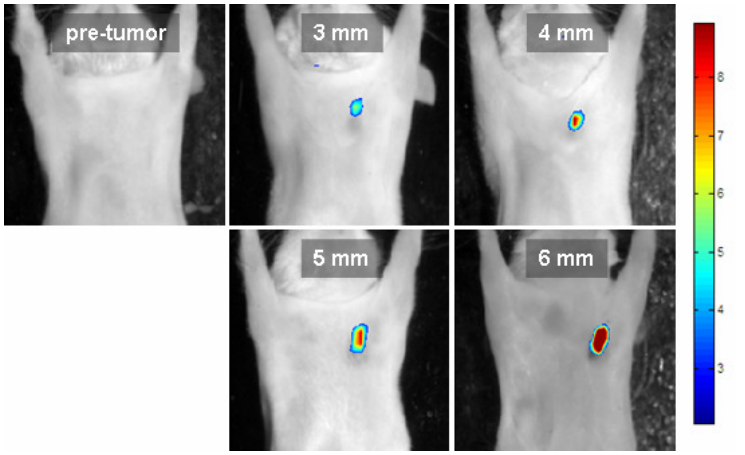


**Figure 10**: A mouse imaged prior to visible manifestation of tumors and subsequently imaged on a weekly basis to follow tumor growth from 3 mm to 6 mm in diameter. The mouse was injected via tail-vein with 2 nmol of a cathepsin-activatable NIR probe 24-hours prior to each imaging session.

performed as part of the algorithmic development performed accurately not just in the case of well controlled phantoms but also *in-vivo*. Tumor growth studies, confirmed against caliper measurements demonstrated accurate delineation of tumor volume. A representative example is shown in Fig.10. Independent tests of the correlation of protease activity in these tumors, further confirmed the quantitative ability of the method. A significantly larger data sample is included in the in-vivo studies, showing a linear trend between protease activity and tumor size / growth.

## AIM 2: IN-VIVO STUDIES

### Transgenic mouse models

We successfully established an MMTVneu transgenic mouse colony (c-neu oncogene; strain name FVB/N-TgN(MMTVneu)202Mul, Jackson Laboratory, Bar Harbor, Maine) for the purposes of these studies as proposed in the grant proposal. In this model, the mouse mammary virus tumor (MMTV) promoter directs expression of the c-neu oncogene to the mammary fat pads. The model was originally reported to develop mammary tumors in 50% of females by 89 days, but ultimately there is 90% penetrance by 5-6 months. The major reason of establishing a colony was to eliminate all availability issues that may arise when requesting such a popular transgenic strain from an outside supplier, expediting the progress of our intended studies. Genotyping results, performed in all animals originally received, confirmed the presence of the neu transgene as shown in Fig.11. Similarly Western blots performed on each tumor imaged (not shown) demonstrated elevated levels of protease activity (cathepsin B,S and MMP 2/9).

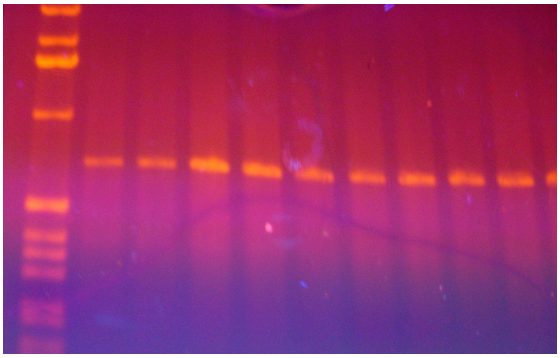

**Figure 11:** Agarose gel displays results of genotyping of MMTVneu transgenic females. PCR was performed using primers designed specifically for the rat Her-2/neu oncogene. The appropriate 600-700 bp neu transgene is present in all animals received.

### In-vivo imaging studies – screening and tumor growth.

Significantly evolved fluorescence imaging studies were achieved in the course of this grant proposal that went beyond the original expectations, due to technological and methodological advances that were achieved in the course of this development. Importantly, dual wavelength imaging allowed not only for resolving a cancer related bio-marker but also in accurate quantification via the co-injection of a vascular probe characterizing tumor angiogenesis and permeability. While this measurement of angiogenesis and permeability is useful metric of tumor growth on its own, it becomes significantly more important as it can independently characterize the bio-distribution of the protease-sensitive molecular probe. Therefore delivery and presence of biomarker can be independently characterized. In total, 16 animals were imaged using single wavelength imaging and 55 animals using dual wavelength imaging. Dual wavelength imaging consisted of the simultaneous injection of 2nmol of an NIR cathepsin-

activatable probe (ProSense, Visen Medical, Woburn, MA) and an NIR vascularization agent (AngioSense, Visen Medical, Woburn, MA) via tail vein 24 hours prior to imaging of transgenic mice bearing developing tumors. The Angiosense is essentially the same molecule as the Prosense, albeit with less fluorochromes loaded to avoid quenching. Therefore the probe is always "on" and allows for visualization of the biodistribution of ProSense which generally activated only in the presence of proteases (cathepsins). Figure 12 demonstrates FMT of a her2/neu mouse bearing a 7mm tumor. The cathepsin-activatable NIR probe shows strong signal selectivity within the region of the tumor, suggesting elevated cathepsin activity at this location (top row). At the same time, the images in the bottom row resulted from FMT of the NIR vascularization agent and clearly indicate increased probe distribution not only within the tumor but throughout the surrounding area, consistent with increased tumor vascularity. Thus inclusion of the fluorescent *in vivo* blood pool imaging agent not only provides reliable, non-invasive imaging of vascularity but also enables quantification of delivery of both probes by serving as an internal control.

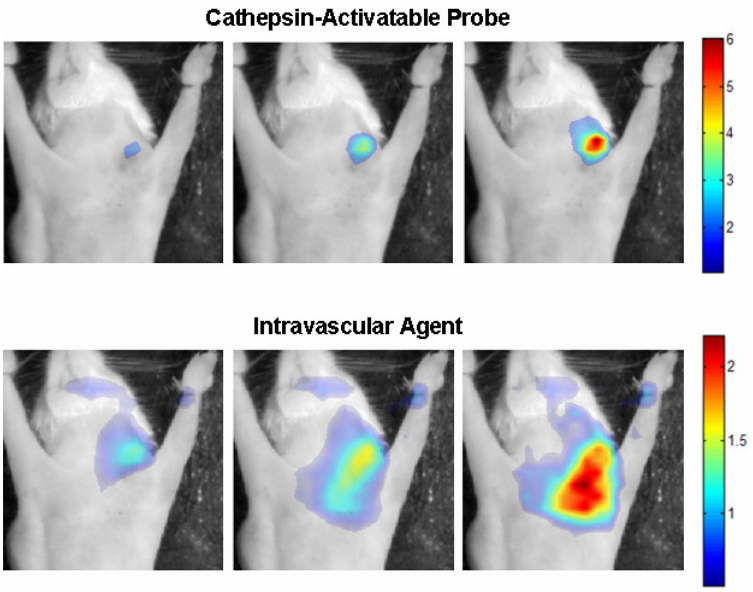


**Figure 12:** Dual wavelength FMT of mouse with 7 mm tumor. **Top row**: FMT of cathepsin-activatable NIR probe shows strong signal selectively within the region of the tumor, indicative of increased cathepsin activity within the tumor and its microenvironment. **Bottom row**: FMT of NIR vascularization agent, showing increased probe distribution not only throughout the tumor but also the surrounding regions, which is consistent with increased tumor vascularity. Note that the measurement of activated cathepsin probe is contained within the measurement of probe bio-distribution, as expected.

The dual wavelength approach can be particularly useful in instances where limited fluorescence activity is recorded from legions of interest. For example, if low activity is recorded in the ProSense channel, the dual wavelength approach can readily identify if this is due to lack of probe delivery and target accessibility or otherwise if it is due to lack of enzymatic activity.

Figure 13 shows a similar imaging session to the one shown in Fig.7 from a different mouse with a tumor grown in the lower left mammary region measuring ~4mm in size. Similarly this MMTVneu female mouse was injected with the NIR vascular contrast agent (AngioSense 750) and the cathepsin activatable (ProSense 680) smart probe 24 hours prior to imaging. In this example we were again able to explore the bio-distribution of the probe through simultaneous detection of the vascular agent. The AngioSense signal may be again noted as extending far

beyond the region of the tumor itself suggesting that an increase in local vasculature has occurred

Statistical analysis of the entire sample revealed that protease related signals can reproducibly resolve tumors as small as ~3mm in diameter. 30 animals entered the screening study and were imaged with a protease-sensitive probe (ProSense probe) and the AngioSense probe in the second spectral channel, whereas another 10 animals were imaged in screening mode for the detection sensitivity achieved when imaging matrix metalloproteinase (MMP's). (15 more animals were imaged for tumor growth and identification of secondary cancers as described later). The results, summarized in the following charts, demonstrated a robust correlation between protease activity (normalized to the Angiosense signal) and tumor growth. Overall tumors as small as 3mm in diameter could be detected based on the protease signatures.

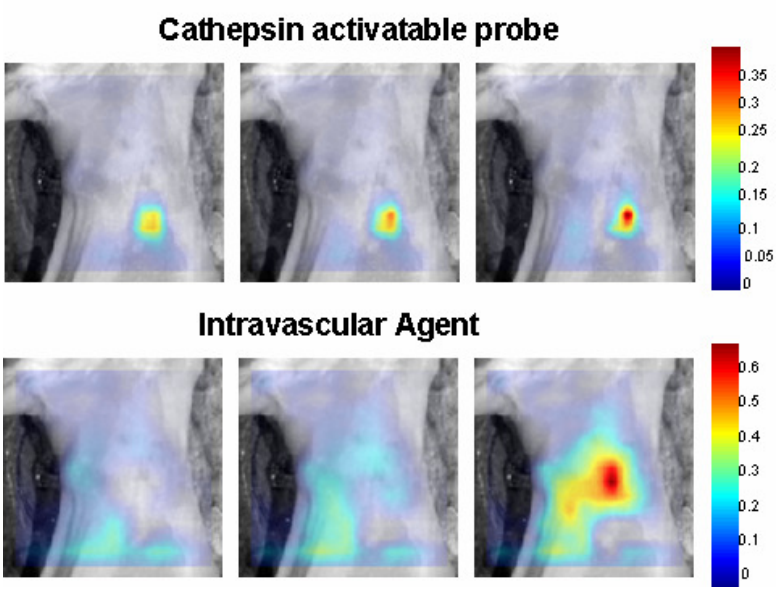


**Figure 13:** FMT of mouse with 4 mm tumor. Similarly to Fig.12 **Top row**: FMT of cathepsin-activatable NIR probe shows strong signal selectively within the region of the tumor, indicative of increased cathepsin activity within the tumor and its microenvironment. **Bottom row**: FMT of NIR vascularization agent, showing increased probe distribution not only throughout the tumor but also the surrounding regions.

All tumor regions above 3mm in diameter were clearly visible in near-infrared images for each probe; with tumor fluorescence being 2.2, 1.6 and 1.8 times higher than background fluorescence measured in non-diseased tissue for Prosense, MMpSense and Angiosense, respectively. While these are generic metrics of the overall performance achieved in the studies, Fig.15 and Fig.16 summarize individual cathepsin- and MMP2/9-resolving studies for individual animal cases. These

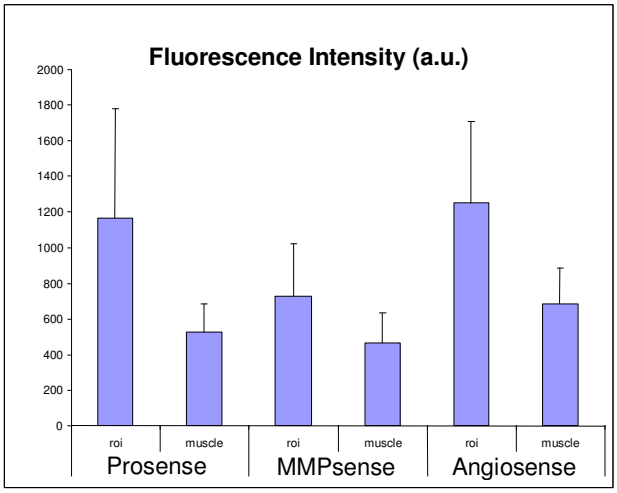


**Figure 14:** In-Vivo NIRF signal measured in Tumor and Muscle for each Probe

figures summarize the major findings in this study, in regard to the sensitivity and differentiation ability of tumors using quantitative fluorescence imaging, while a significant number of additional analyses have been performed and are prepared for publication.

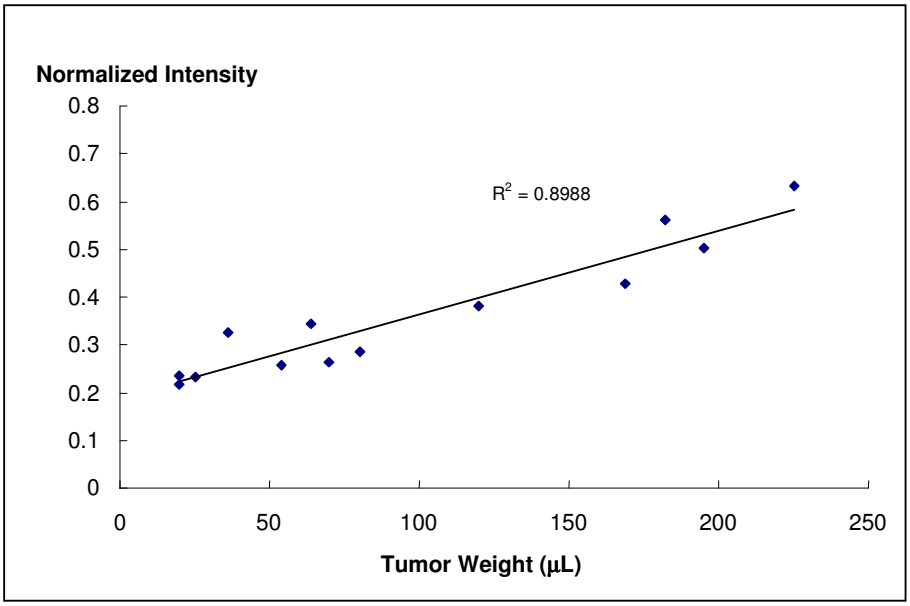


**Figure 15.** Cathepsin expression normalized to fluorescent probe bio-distribution (i.e. vascularization and permeability)

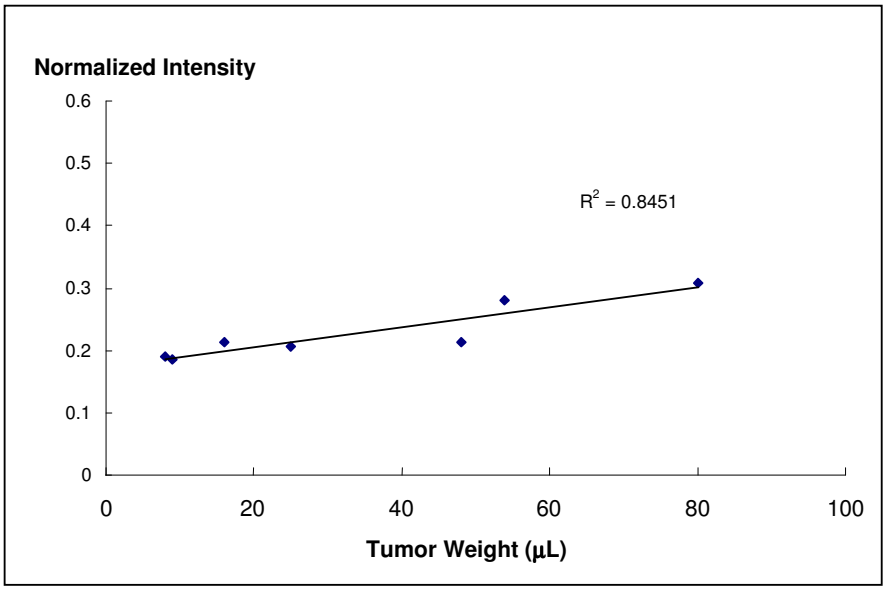


**Figure 16.** Matrix metalloproteinase expression normalized to fluorescent probe bio-distribution (i.e. vascularization and permeability)

First, cathepsin-based tumor detection yielded brighter fluorescence signals compared to MMP-based differentiation. Second, a linear correlation is observed between the fluorescence signal observed and tumor volume. This is generally expected as increased tumor volume will contain more fluorescence probe. Importantly however these are normalized signals to the tumor vascular volume fraction and permeability, therefore they reflect true protease up-regulation with tumor volume, not simply the result of fluorochrome pooling in the tumor. Overall, despite considerable tumor heterogeneity in terms of intra-tumoral fluorescence distribution, fluorescence signals measured in tumor region of highest protease expression (using manually drawn regions of interest ROI's) yield very similar results to analysis performed by taking ROI's at the entire tumor volume. This observation held for both Cathepsin and MMP signals.

Regarding *early detection* of tumor development, our final data analyses indicated considerable capacity for successful identification of tumors as small as 3-4mm in diameter ( ~ 50μL see Fig.15, 16). The findings suggest that for tumors smaller than this metric, no significant protease activity exists to produce detectable signals. The contrast achieved varied significantly from 1.6 for the smaller range of tumors to more than 3-fold in some larger tumors.

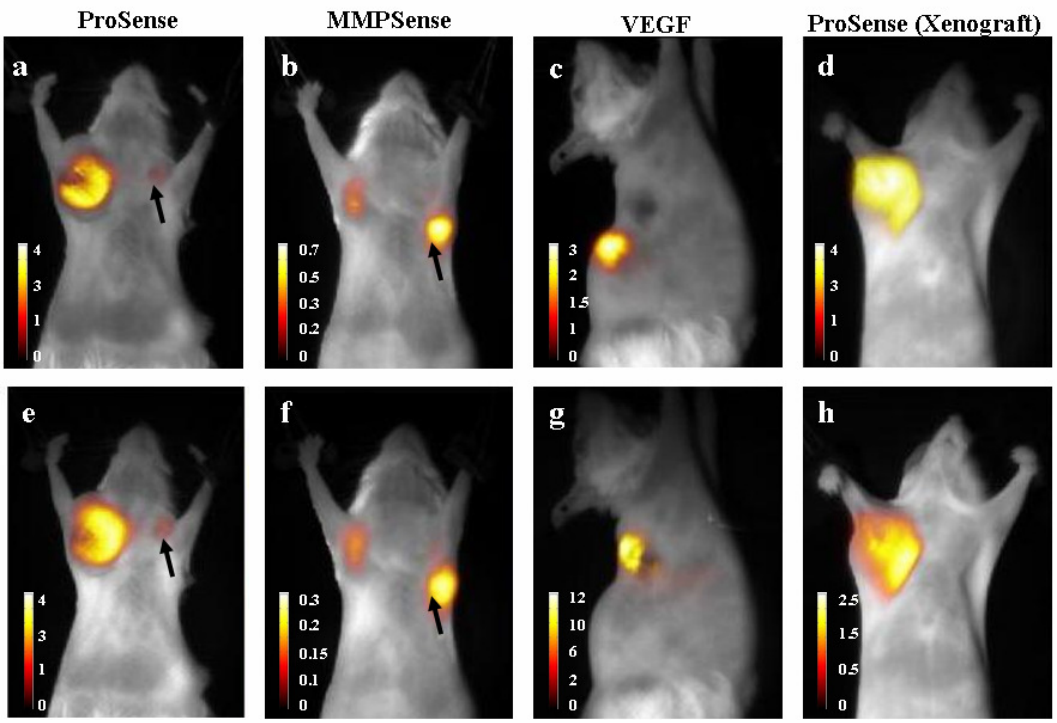


**Figure 17:** Her-2 transgenic mouse bearing 10mm$^2$ upper right and 5mm$^2$ upper left mammary tumors imaged with ProSense (a) and AngioSense (e), Her-2 transgenic mouse bearing 5mm$^2$ upper right and 3mm$^2$ upper left mammary tumors imaged with MMPSense (b) and AngioSense (f), Her-2 transgenic mouse bearing 3mm$^2$ abdominal mammary tumor imaged with VEGF probe (c) and AngioSense (g), MDA-MB 231 tumor cell xenograft model bearing 10mm$^2$ upper right mammary tumor imaged with ProSense (d) and AngioSense (h).

.

Next, beyond consideration of the sensitivity of our approach for detection of the onset of tumor formation, we also evaluated tumor development over time as a function of protease activity, vascular volume, etc. in a number of individual mice over a course of several weeks. This was done in the interest of monitoring *disease progression* and evaluating the extent of the appearance of secondary foci or metastatic disease. Similarly, a number of different probes were employed so as to address various parameters of tumor growth and development, i.e. we gauged again the activity of a variety of cysteine proteases (cathepsin B, L, etc) and matrix metalloproteinases (MMP 9, 2, etc.) as well as the accessibility of targeting the vascular endothelial growth factor receptor at the tumor location (figure 17a-d; and appended poster presentattion). In particular, figures 17 a, b also indicate the potential for detection of secondary tumor locations (black arrows), visualized following a primary tumor, which were 3-5mm in diameter (upon the follow-up examination). In the case of the mouse probed with MMPsense in 2b, the $3mm^2$ secondary tumor may be noted as exhibiting nearly twice the level of protease activity as that observed in the larger primary tumor ($5mm^2$). The animals represented in figure 17, were simultaneously evaluated for overall success of probe delivery to the tumor site/s through observation of the distribution of the accompanying intravascular agent (AngioSense) within the developing vasculature surrounding the regions of interest (figure 17 e-h). In this way, we were able to acquire a most accurate indication of the general profile of the respective biomarker with confirmation of its potential for distribution to the given tumor in each animal. Observations on 15 animals demonstrated nearly identical findings.

To further improve early detection, we further investigated in a pilot study the ability of targeted, antibody based probes; in this case the Her-2 antibody conjugated to Cy5.5, also injected into a transgenic mouse 24-hours prior to imaging. In this case, fluorescence imaging was able to resolve tumors as small as 1 mm tumor (n=3; tumors measured across their apparent diameter using calipers; see Figure 18). This finding demonstrates selective probe bio-distribution at early stages of disease progression and represents a significant achievement toward the goal of early detection. While antibody based detection was not part of the original aims of this proposal, this study can serve as preliminary results to showcase the potential for even more sensitive detection, beyond the 3mm limit identified for protease based probes.

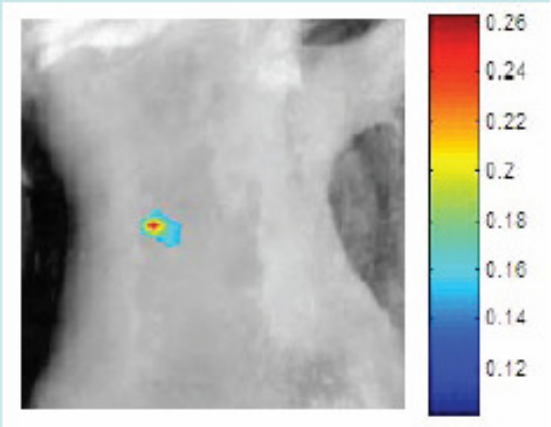


**Figure 18:** Tomographic slice (z = 1.28 cm) revealing a 1 mm tumor in the right mammary fat pad of mouse

## AIM 3: CLINICAL TRANSLATION

### Breast Imaging Phantoms

We researched two manufacturing methods for developing diffusing phantoms that can be fluorescing and these methods are now in press [35]. Specifically, silicone rubber and polyester casting resin are used as base materials, and silicone pigments and $TiO_2$ / India Ink are added to vary the optical properties (scattering and absorption), respectively. Fluorophores are then added to the silicone and resin, if the phantom is to be made fluorescent, and solidifying agents are added to cure the samples. Hydrophobic (IR-780 Iodide) and hydrophilic (Cy5.5) fluorophores were tested successfully in the silicone and resin standards, respectively. Photograph of one phantoms constructed can be seen in Fig.19. Analytical details are presented in Ref. [35].

Quantification of the phantom's optical properties has been done using time-resolved methods. In short, a wavelength tunable femto-second laser (MaiTai, Spectra-Physics, Mountain View, California) with a pulsewidth of approximately 100 fs was coupled to a scanning galvanometer. The laser light could be scanned in a non-contact manner across a sample as desired. The transmitted light was detected with a Cooke SensiCamQE CCD camera coupled with a gated image intensifier (LaVision Picostar HR12, LaVision GmbH, Goettingen, Germany). A high-rate imager (Kentech Instruments Ltd., Oxfordshire, England) and a picosecond delay unit (Kentech) allowed acquisition of images with gate widths of 200 ps with a temporal step size of 25 ps.

**Figure 19.** Silicon breast phantom constructed

Using computer software, the images can be analyzed to yield multiple photon-profile curves as a function of time and radial position from the source. By fitting these curves with the time-dependent diffusion equation, the optical coefficients can be obtained with high accuracy. Thus, by varying the concentration of one particle in the sample while holding the concentration of the other particle constant, a relationship between the particle concentration and the respective optical coefficient can be determined. These relationships were then used for determining the necessary amount of each particle to add. An example is shown below.

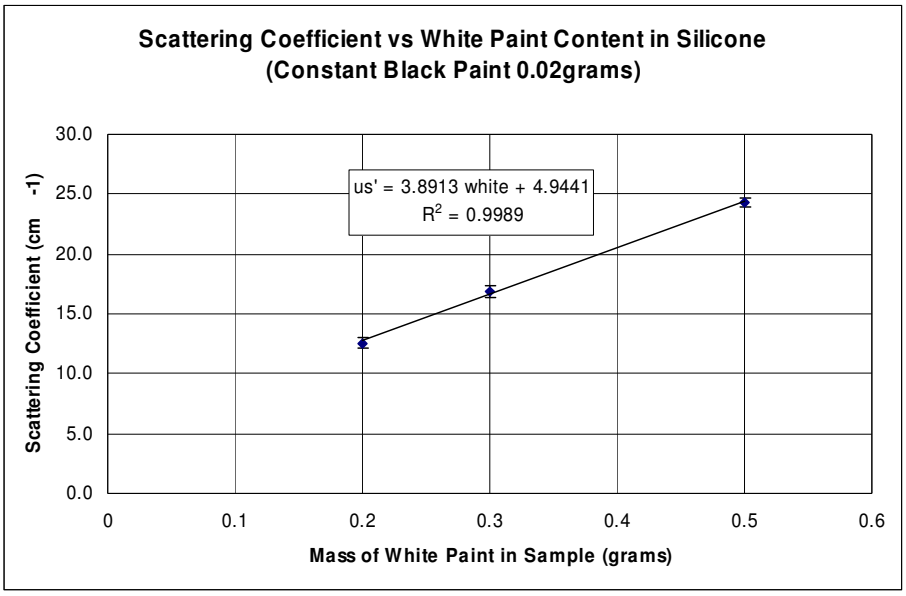


**Figure 20:** Relationship between the mass of white paint added to a silicone sample and the scattering coefficient. Typical human breast values for the reducced scattering coeeffcient are ~10 – 15cm-1.

Using such phantoms, manufactured at appropriate sizes, shapes and varying optical properties, we constructed breast simulating solid phantoms of various dimensions (6-10cm thickness, assuming a gently compressed breast). These phantoms were drilled with appropriate openings in which fluorescent inserts simulated the background tumor. Importantly, phantoms were made fluorescent and the fluorescent insert was appropriately engineered in volumes and contrast as found from the in-vivo mouse studies.

**Phantom measurements and simulations**

Clinical fluorescent imaging would require detection of fluorescent signals that have propagated for several centimeters into tissue. Fig 21 demonstrates the photon attenuation rate of different human tissues at 690 nm. It is shown that breast tissue and the adult lung attenuates NIR light one order of magnitude every 4 cm, the attenuation rate in denser breast and muscle approaches one order of magnitude every 3 cm and the attenuation rate in brain tissue is approximately one order of magnitude every 1.5 cm [36]. In terms of signal-strength, fig.21 plots fluorescence counts per second of exposure and $mm^2$ of CCD detector area, as a function of organ diameter. This calculation is for a tumor-like lesion of 100μL volume and 100nM of Cy5.5 concentration (10 pico-moles) located near the center of the various organs simulated. The simulation is based on experimental measurements obtained from a diffuse volume (similar to the one shown on fig. 22a but with varying outer diameter) using 30mW of illuminating power. The 10dB, 20dB and 30dB signal to noise (SNR) level achieved assuming shot-noise limited detection is also shown. This result indicates that fluorescence signals could be detected after propagation for several centimeters into tissue, which could potentially allow clinical imaging of fluorescent probes [36].

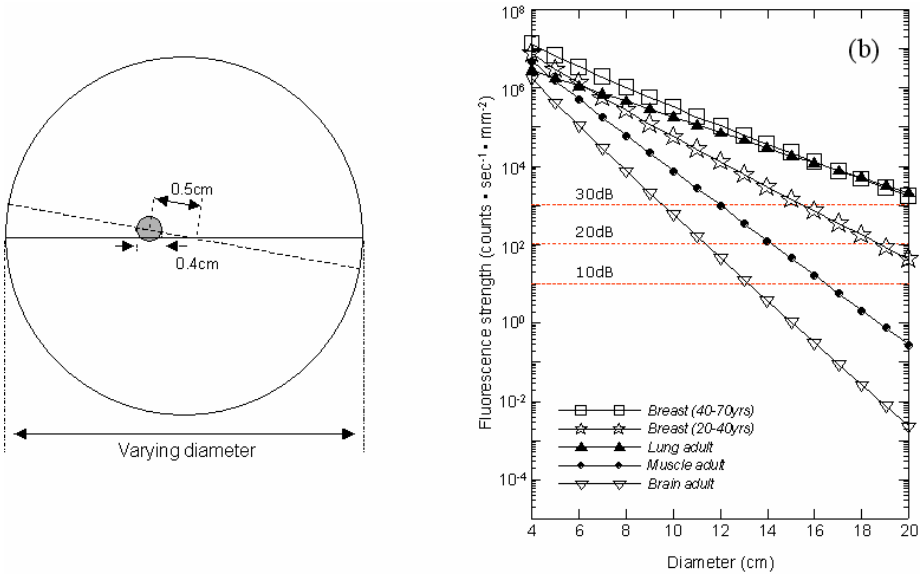


**Figure 21**: a) Average fluorescent photon counts expected at the periphery of the breast (and other organs) as a function of diameter due to a fluorochrome located 0.5cm off center as shown in the schematic on the left. Three SNR levels for shot-noise limited detection are also plotted to indicate detection limits.

This simulation approach was then employed to examine clinical detection based on the signals obtained in-vivo from the animal studies. We assumed tumors of different sizes with the corresponding fluorescence concentration activity resolved in-vivo (50 – 200 nM) and the background fluorescence recorded. The simulation assumed average optical properties for the breast, i.e. absorption coefficient of 0.4 cm-1 and reduced scattering coefficient of 12cm-1. The key results are summarized on Fig. 22. In particular it is shown that the minimum lesion that can be detected largely depends on the level of background fluorescence achieved. At the absence of background fluorescence, lesions as small as 4mm in diameter can be detected, however as non-specific accumulation of fluorochrome may appear the sensitivity may significantly vary. Therefore methodologies that minimize background accumulation are essential for highly sensitive molecular-based detection in clinical breast cancer detection. This is reflected in Fig.22 whereas three levels of background fluorescence are depicted, showing a rapid decrease in minimum lesion detected as the background fluorescence diminishes. In-vivo measurements revealed that background fluorescence in mice is of strength corresponding to ~20nM of equivalent Cy5.5 dye. We note that measurements of background fluorescence from mice do not reflect the clinical case scenario for human breast imaging. This is because the mouse measurement incorporate several diverse structures and organs, such as the heart, lung, muscle etc, which are different that the common adipose and parenchymal tissues seen in the breast. Accurate background fluorescence measurements can only be obtained by clinical measurements. Therefore the "background fluorescence" offsets shown in Fig.22 are only indicative of the overall behavior of the technology.

Breast phantoms were then constructed using scattering resin material with controlled absorption and fluorescence properties, as shown in Fig.23. The phantoms were made of

background optical properties as found in mice in-vivo (background fluorescence strength corresponding to 10-20nM of Cy5.5 fluorescence dye). Measurements of detection sensitivity and overall imaging were performed by immersing the phantoms in matching fluid after machining them to different thicknesses, i.e. 6cm and 8cm, which are common thicknesses for the gently compressed breast (see Ref.??). The minimum detected fluorescent legions for three different phantoms are also shown on Fig.22 as black stars, closely confirming the experimental observations. Varying in volume lesions were examined in each case, by injecting a larger amount of fluorochromes in drilled opening in the phantom. In all cases a worse case scenario was assumed, for volumes close to the center of the phantom. Correspondingly the fluorescence concentrations of the fluorochromes that were used to simulate tumors were 150nM in concentrations for lesions corresponding to 50-150micro-L lesions and 250nM for larger volumes. These properties were average properties found in-vivo in the animal measurements.

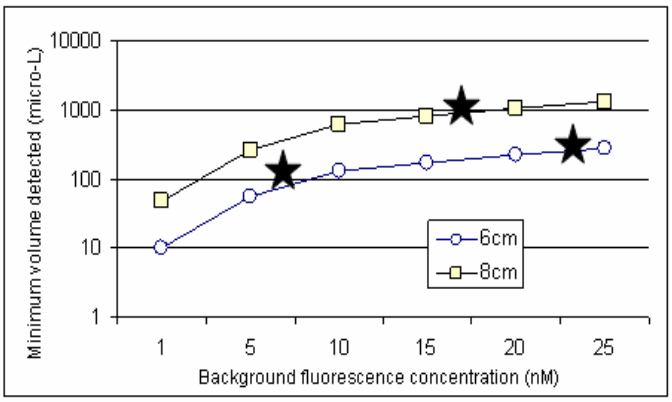


**Figure 22**: Simulations shown that an increase in background fluorescence significantly limits the minimum lesion that can be detected through the human breast. Measurement assumed breast of 6 and 8 cm thickness gently compressed between two parallel plates. Black stars correspond to experimental determination of minimum lesion volume detected from phantom measurements. In all cases 150nM of Cy5.5 has been assumed or added in the fluorescence lesions.

The above simulations used properties found in-vivo from the animal measurements and propagated them to the clinical case using simulations and phantoms. Simulations utilized models based on the diffusion equation using average optical properties (and thus attenuation) for breast tissue. It has been shown that breast hererogeneity does not affect image reconstruction in fluorescence tomography based on the normalized Born approximation [30]. Therefore the observations herein accurate reflect overall performance in the human breast, even if homogenous models of photon propagation have been assumed.

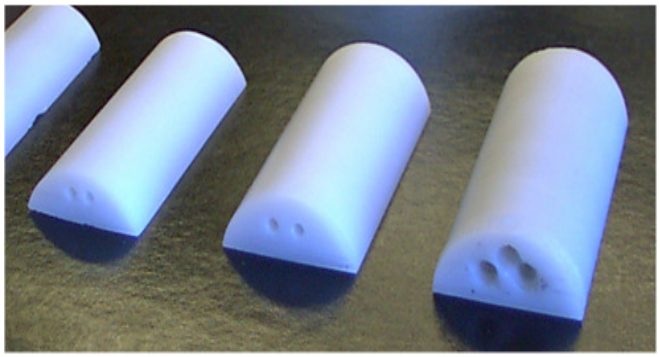

**Figure 23.** Solid phantoms simulating the human breast were constructed in various shapes and sizes. The phantoms contained openings so that tumors of various concentrations could be simulated.

## SUMMARY AND CONCLUSION

This study is perhaps the first such examination of the clinical utility of fluorescence molecular probes for breast cancer detection. To accurately address in-vivo considerations, this work focused a large part of the development to establish breast cancer animal models of spontaneous disease, using transgenic animal models. Compared to mouse xenographs, the Her2/neu model utilized herein is expected to more closely resemble human breast cancer development and present more realistic barriers in probe bio-distribution. As such it represent an accurate pre-clinical step towards clinical translation of fluorescence breast cancer imaging.

A considerable portion of this development further focused on delivering an imaging method that takes into account the non-linearity associated with photon propagation in tissue and with heterogeneous optical properties, as those found in tissues *in-vivo*. The methodology developed offers a quantitative and high-fidelity imaging modality appropriate not only for small animal imaging but also for human breast imaging as well. Imaging of non-specific fluorochromes through the human breast had been previously shown by the PI of this proposal [15]. The work herein represents an important step towards practical molecular imaging of breast cancer in-vivo as it achieved two major milestones. The first was the use of molecular probes in breast cancer detection, in particular cathepsin- and matrix-metlaloproteinase- sensitive fluorescent molecules that could be also used clinically. This is the first time that pre-clinical imaging of such probes has been performed in a clinically relevant study. The second milestone achieved was the quantitative assessment of the utility of these probes *in-vivo*. Quantification was achieved only via the methodology developed in this proposal, utilizing tomographic principles and accurate models of photon propagation in tissues. Further key development such as simultaneous imaging of molecular target and probe bio-distribution yielded an unprecedented level of accuracy and fidelity for fluorescence imaging applications.

To reach closer to conclusions for clinical translation, simulations were performed for the clinical case in order to outline the clinical utility of the method, given the in-vivo findings on the animal models. Overall it was found that lesions of 5-7mm in size can be detected through the human breast, based on protease signals, assuming background fluorescence of equivalent strength to 10nM cy5.5 while higher background fluorescence reduces the size of the lesion that can be detected. This prediction is for the gently compressed human breast, between two parallel plates, to 6-8cm thickness and for the Cy5.5 or Cy7 dye. Protease markers are generic caner markers that can be applied to virtually all of breast cancers. Their specificity however may be reduced as they can be also activated in inflammatory, non cancerous lesions as well. To increase specificity but also potentially detection sensitivity we performed pilot studies with other bio-markers as well, for example VEGF or other endothelial markers or estrogen receptors. In this particular cancer model the herceptin antibody proved efficient in findings even micro-cancer foci, even if 100% compatibility is expected between human herceptin and the animal receptor. We expect this to be a field receiving increasing attention, i.e. the identification of appropriate bio-markers for improving detection or treatment monitoring in breast cancer. Regardless, the particular biomarkers studied herein, i.e. particular cathepsin (B,S,L) and MMP 2/9 showed that reliable detection can be expected in lesions that are difficult to currently detect with standard

mammography procedures, while imparting the potential for increased specificity, since detection is based on a particular cancer biomarkers and not generic anatomical changes.

## Key Research Accomplishments – Year 1

- Implementation of a system that combines 4 modes of illumination/detection namely reflectance, transillumination tomosynthesis and tomography for use in years 2 & 3
- Construction of appropriate phantoms for testing imaging performance.
- Establishment of appropriate animal breast cancer models.
- Establishment of sensitivity limits for the detection of fluorochromes of better than 10nM in 200μL volumes in the center of phantoms with breast optical properties.
- Establishment that tomographic methods are superior to planar imaging methods as a function of depth, optical properties and heterogeneity and is the method of choice for subsequent studies in years 2 & 3. Planar imaging methods will be important for scout studies, where quantification will be necessarily obtained from tomography or tomosynthesis.
- Development of algorithms that are insensitive to background fluorescence and heterogeneity.
- In-vivo imaging of the first animals with spontaneous breast cancer using protease activatable probes to detect cancer

## Key Research Accomplishments – Year 2

- Establishment of own MMTVneu transgenic mouse colony and expansion to additional providers of appropriate animal models in interim.
- Diversification to orthotopic implants of human mammary cell lines
- Development of multi-spectral imaging analyses for improving the accuracy of the observation and providing internal controls.
- Development of automatic – threshold statistical methods for inversion to eliminate user input and thus standardize quantification.
- Imaging of 16 animals in single wavelength and 9 animals in dual wavelength studies.
- Construction breast-like phantoms

## Key Research Accomplishments – Year 3

- Confirmation of animal models using genotyping
- Imaging of another 55 animals using dual-wavelength imaging employing probes revealing major cathepsins (B,S, L) and matrix metalloproteinases 2/9.

- Histological confirmation of samples and characterization of protease content by Western blots.
- Statistical analysis of findings to yield performance as a function of tumor growth and tumor size.
- Identification of minimum detection limits based on protease signals.
- Construction of breast like phantoms and experimental measurements of minimum lesion detected

# Reportable Outcomes Yr 1 & 2

**Ntziachristos V**, Turner G, Dunham J, Windsor S, Soubret A, Ripoll J & Shih HA, "Planar fluorescence imaging using normalized data" J. Biomed. Optics 10(6): 064007 (2005).

Soubret A, Ripoll J, **Ntziachristos V** , "Accuracy of fluorescent tomography in presence of heterogeneities: Study of the normalized Born ratio", IEEE Med. Imag. **24**(10): 1369-1376 (2005).

Hyde D, Miller E, Brooks DH, **Ntziachristos V,** "A Statistical Approach to Inverting the Born Ratio", IEEE Trans. Med. Imag. May 2007

Dunham J, Soubret A, & **Ntziachristos V**, "Dual wavelength fluorescence molecular tomography of breast cancer in Her2/neu mice" in preparation

Soubret A, Turner G, **Ntziachristos V** , "Fluorescent molecular tomography in presence of background fluorescence, Phys. Med. Biol. **51**: 3983-4001 (2006).

Lasser T, **Ntziachristos V**. "Optimization of 360 degrees projection fluorescence molecular tomography" Med Image Anal. Apr 19 (2007).

Baeten J., Niedre M., Dunham J., **Ntziachristos V**., Development of fluorescent materials for Diffuse Fluorescence Tomography standards and phantoms Opt. Express in press (2007)

Lasser T, Deliolanis N, **Ntziachristos V**. "Surface Reconstruction for free-space 360° Fluorescence Molecular Tomography and the effects of animal motion" IEEE Trans. Med. Imag. in press (2007).

Haller J., Deliolanis N., **Ntziachristos V**., Imaging protease biomarkers in breast cancer in prep.

Haller J., Baeten J., **Ntziachiristos V.,** Multi-spectral fluorescence molecular tomography improves the accuracy of fluorescence molecular imaging in press

Haller J, **Ntziachristos V.,** In vivo Visualization of Breast Cancer Biomarkers by Fluorescence Spectral Imaging., Dana-Farber Workshop on Cancer Research, Boston MA 2007.

Shih H, **Ntziachristos V.,** "In vivo Characterization of Her-2/neu Carcinogenesis in Mice Using Fluorescence Molecular Tomography". Optical Society of America Topical Meeting on Biomedical Optics, Ft. Lauderdale, MI (2006)

Windsor SD, Shih HA, and Ntziachristos, V, "In-vivo fluorescence molecular tomography of mammary adenocarcinomas in transgenic mice bearing an activated c-neu oncogene," U.S. Army Era of Hope Conference, Philadelphia, PA, June 2005.

Windsor SD, Shih HA, Weissleder R, Ntziachristos V, "Simultaneous imaging of protease expression and biodistribution in Her-2/neu mice using dual-wavelength fluorescence molecular tomography," Society of Molecular Imaging Conference, Cologne, Germany, Sept. 2005.

# References


[1] Humphrey LL, Helfand M, Chan BKS, and e. al., "Breast cancer screening: a summary of evidence for the U.S. preventive services task force.," *Annals of Internal Medicine,* vol. 137, pp. 347-60, 2002.

[2] Fletcher SW and E. JC., "Clinical practice. Mammographic screening for breast cancer.," *N Engl J Med,* vol. 348, pp. 1672-80, 2003.

[3] Arriagada R., Le M. G., Contesso G., Guinebretiere J. M., Rochard F., and S. M., "Predictive factors for local recurrence in 2006 patients with surgically resected small breast cancer," *Ann. Onc.,* vol. 13, pp. 1404 - 1413, 2002.

[4] Arriagada R, Le MG, Rochard F, and C. G., "Conservative treatment versus mastectomy in early breast cancer: patterns of failure with 15 years of follow-up data. Institut Gustave-Roussy Breast Cancer Group.," *J Clin Oncol,* vol. 14, pp. 1558-1564, 1996.

[5] Mirza NQ, Vlastos G, Meric F, Buchholz TA, Esnaola N, Singletary SE, Kuerer HM, Newman LA, Ames FC, Ross MI, Feig BW, Pollock RE, McNeese M, Strom E, and H. KK., "Predictors of locoregional recurrence among patients with early-stage breast cancer treated with breast-conserving therapy.," *Ann Surg Oncol.,* vol. 9, pp. 256-65, 2002.

[6] Wallgren A, Bonetti M, Gelber RD, Goldhirsch A, Castiglione-Gertsch M, Holmberg SB, Lindtner J, Thurlimann B, Fey M, Werner ID, Forbes JF, Price K, Coates AS, and C. J, "Risk factors for locoregional recurrence among breast cancer patients: results from International Breast Cancer Study Group Trials I through VII.," *J Clin Oncol.,* vol. 21, pp. 1205-1213, 2003.

[7] R. Weissleder and U. Mahmood, "Special review: Molecular imaging," *Radiology,* vol. 219, pp. 316-333, 2001.

[8] R. Weissleder and V. Ntziachristos, "Shedding light onto live molecular targets," *Nat Med,* vol. 9, pp. 123-8, Jan 2003.

[9] V. Ntziachristos, J. Ripoll, L. H. V. Wang, and R. Weissleder, "Looking and listening to light: the evolution of whole-body photonic imaging," *Nature Biotechnology,* vol. 23, pp. 313-320, Mar 2005.

[10] V. Ntziachristos, E. A. Schellenberger, J. Ripoll, D. Yessayan, E. Graves, A. Bogdanov, L. Josephson, and R. Weissleder, "Visualization of antitumor treatment by means of fluorescence molecular tomography with an annexin V-Cy5.5 conjugate," *Proceedings Of The National Academy Of Sciences Of The United States Of America,* vol. 101, pp. 12294-12299, Aug 17 2004.

[11] S. B. Colak, M. B. van der Mark, G. W. Hooft, J. H. Hoogenraad, E. S. van der Linden, and F. A. Kuijpers, "Clinical optical tomography and NIR spectroscopy for breast cancer detection," *Ieee Journal of Selected Topics in Quantum Electronics,* vol. 5, pp. 1143-1158, 1999.

[12] D. J. Hawrysz and E. M. Sevick-Muraca, "Developments toward diagnostic breast cancer imaging using near-infrared optical measurements and fluorescent contrast agents," *Neoplasia,* vol. 2, pp. 388-417, 2000.

[13] B. Pogue, S. Poplack, T. McBride, W. Wells, K. Osterman, and U. Osterberg, "Hemoglobin imaging of breast tumors with near-infrared tomography.," *Radiology,* vol. 214, p. G05H, 2000.
[14] V. Ntziachristos and B. Chance, "Probing physiology and molecular function using optical imaging: applications to breast cancer," *Breast Cancer Res,* vol. 3, pp. 41-46, 2001.
[15] V. Ntziachristos, A. G. Yodh, M. Schnall, and B. Chance, "Concurrent MRI and diffuse optical tomography of breast after indocyanine green enhancement," *Proc. Natl. Acad..Sci. U.S.A.,* vol. 97, pp. 2767-72, 2000.
[16] E. Graves, J. Ripoll, R. Weissleder, and V. Ntziachristos, "A Sub-Millimeter Resolution Fluorescence Molecular Imaging System for Small Animal Imaging," *Medical Physics,* vol. 30, pp. 901-911, 2003 2003.
[17] R. Weissleder, C. H. Tung, U. Mahmood, and A. Bogdanov, "In vivo imaging of tumors with protease-activated near-infrared fluorescent probes," *Nature Biotech,* vol. 17, pp. 375-8, 1999.
[18] C. H. Tung, "Fluorescent peptide probes for in vivo diagnostic imaging," *Biopolymers,* vol. 76, pp. 391-403, 2004.
[19] C. H. Tung, "Developing fluorescence probes for in vivo molecular imaging," *Abstracts Of Papers Of The American Chemical Society,* vol. 227, pp. U146-U146, Mar 28 2004.
[20] J. E. Koblinski, M. Ahram, and B. F. Sloane, "Unraveling the role of proteases in cancer," *Clin Chim Acta,* vol. 291, pp. 113-35., 2000.
[21] Levicar N, Kos J, Blejec A, and e. al., "Comparison of potential biological markers cathepsin B, cathespin L, stefin A and stefin B wth urokinase and plasminogen activator inhibitor-1 and clinicopathological data of breast carcinoma patients.," *Cancer Detect Prev,* vol. 26, pp. 42-9, 2002.
[22] S. Yan, M. Sameni, and B. F. Sloane, "Cathepsin B and human tumor progression," *Biol Chem,* vol. 379, pp. 113-23, 1998.
[23] V. Ntziachristos, G. Turner, J. Dunham, S. Windsor, A. Soubret, J. Ripoll, and H. Shih, "Planar fluorescence imaging using normalized data," *Journal of Biomedical Optics,* vol. 10, p. 064007, 2005.
[24] A. Soubret and V. Ntziachristos, "Fluorescence molecular tomography in the presence of background fluorescence," *Phys. Med. Biol.,* vol. 51, pp. 3983-4001, 2006.
[25] A. Soubret, J. Ripoll, and V. Ntziachristos, "Accuracy of fluorescent tomography in the presence of heterogeneities: Study of the normalized Born ratio.," *IEEE Transactions on Medical Imaging.,* vol. 24, pp. 1377-1386, 2005.
[26] T. Lasser, A. Soubret, and V. Ntziachristos, "Surface Reconstruction for free-space 360° Fluorescence Molecular Tomography and the effects of animal motion.," *IEEE Transactions on Medical Imaging,* 2007.
[27] J. Ripoll, V. Ntziachristos, R. Carminati, and M. Nieto-Vesperinas, "Kirchhoff approximation for diffusive waves," *Phys Rev E,* vol. 64, p. 051917., 2001.
[28] J. Ripoll, M. Nieto-Vesperinas, R. Weissleder, and V. Ntziachristos, "Fast analytical approximation for arbitrary geometries in diffuse optical tomography," *Optics Letters,* vol. 27, pp. 527-529, Apr 1 2002.

[29] J. Ripoll and V. Ntziachristos, "Imaging scattering media from a distance: Theory and applications of noncontact optical tomography," *Modern Physics Letters B,* vol. 18, pp. 1403-1431, Dec 20 2004.

[30] V. Ntziachristos and R. Weissleder, "Experimental three-dimensional fluorescence reconstruction of diffuse media using a normalized Born approximation," *Optics Letters,* vol. 26, pp. 893-895, 2001.

[31] D. Hyde, E. Miller, D. Brooks, and V. Ntziachristos, "The statistical inversion of the normalized Born ratio," *IEEE Transactions on Medical Imaging,* vol. in press, 2006.

[32] D. Hyde, E. Miller, D. Brooks, and V. Ntziachristos, "The statistical inversion of the normalized Born ratio," *IEEE Transactions on Medical Imaging,* vol. in press, 2007.

[33] M. J. Eppstein, F. Fedele, J. Laible, C. Zhang, A. Godavarty, and E. M. Sevick-Muraca, "A comparison of exact and approximate adjoint sensitivities in fluorescence tomography," *Ieee Transactions On Medical Imaging,* vol. 22, pp. 1215-1223, Oct 2003.

[34] M. J. Eppstein, D. J. Hawrysz, A. Godavarty, and E. M. Sevick-Muraca, "Three-dimensional, Bayesian image reconstruction from sparse and noisy data sets: Near-infrared fluorescence tomography," *Proceedings Of The National Academy Of Sciences Of The United States Of America,* vol. 99, pp. 9619-9624, Jul 23 2002.

[35] J. Baeten, M. Niedre, J. Dunham, and V. Ntziachristos, "Development of fluorescent materials for Diffuse Fluorescence Tomography standards and phantoms. ," *Optics Express,* vol. in press, 2007.

[36] V. Ntziachristos, J. Ripoll, and R. Weissleder, "Would near-infrared fluorescence signals propagate through large human organs for clinical studies," *Optics Letters,* vol. 27, pp. 333-335, 2002.